Space Science Reviews (2023) 219:21
https://doi.org/10.1007/s11214-023-00970-2

Update of ICON-FUV hmF2 and NmF2 Comparison with External Radio Observations

Gilles Wautelet[1] · Benoît Hubert[1] · Jean-Claude Gérard[1] · Thomas J. Immel[2] · Harald U. Frey[2] · Farzad Kamalabadi[3] · Ulas Kamaci[3] · Scott L. England[4]

Received: 31 December 2022 / Accepted: 9 March 2023
© The Author(s), under exclusive licence to Springer Nature B.V. 2023

Abstract
The Far Ultraviolet Imaging Spectrograph (FUV) onboard the NASA-ICON spacecraft has been providing nighttime O^+ density profiles over mid- and low-latitude since December 2019. These profiles are compared to electron density profiles provided by GNSS radio-occultations and ground-based ionosondes, mainly at the F-peak level where both density and height are compared. This work is an important update of the earlier study published by Wautelet et al. (J. Geophys. Res. Space Phys. 126(11):e2021JA029360, 2021) for two reasons: First, several methodological improvements have been implemented at the calibration and inversion levels. Second, the present work relies on an extended time range, ranging from December 2019 to August 2022, covering therefore periods of increased solar activity, which was not the case for the previous work. It is found that the peak density and height are, on average, similar to radio-based observations by about 10% in density and 7 km in height, meaning that FUV provides peak characteristics compatible with existing ionospheric datasets based on radio signals. However, comparisons of FUV and radio-occultation profiles have to be considered very carefully due to the potentially large difference in the observation geometry, which can account for large density discrepancies even between profiles being closely located and mostly simultaneous. This is particularly important around the crests of the equatorial anomaly where the largest density discrepancies have been observed. In addition, this study highlights the variability of the FUV profiles at the bottomside level, with the analysis of cases where rather large density values were observed while small density values are expected. The latter observation does nevertheless not impact the statis-

The Ionospheric Connection Explorer (ICON) Mission: First Results
Edited by David E. Siskind and Ruth S. Lieberman

✉ G. Wautelet
gilles.wautelet@uliege.be

1 Laboratory of Planetary and Atmospheric Physics, Liège University, Allée du Six Août, 19C, Liège, Belgium

2 Space Sciences Laboratory, University of California, Berkeley, CA, United States

3 Electrical & Computer Engineering, University of Illinois, Urbana Champaign, IL, United States

4 Aerospace & Ocean Engineering, Virginia Tech, Blacksburg, VA, United States

Published online: 28 March 2023

tics concerning the F-peak characteristics, which show that FUV reliably monitors the peak density and height with an accuracy compatible to that of external data sources.

Keywords ICON · Far ultraviolet imager · F-peak · Ionosondes · Radio-occultation

1 Introduction

The Ionospheric CONnection Explorer (ICON) spacecraft was launched on October, 10 2019 and has provided operational measurements of the Earth's ionosphere since December 2019. More specifically, the Far Ultraviolet Imaging Spectrograph (FUV) instrument monitors the ultraviolet airglow at two wavelengths: the atomic oxygen doublet at 135.6 nm and the N_2 Lyman-Birge-Hopfield (LBH) band near 157 nm (Mende et al. 2017). During nighttime, only the OI–135.6 nm emission is measured to provide limb and sub-limb airglow measurements, which are in turn converted into two different scientific data products. While the sub-limb images are co-added using the Time Delay Integration technique (Mende et al. 2022) to accurately map the oxygen emission, the limb profiles are inverted to produce O^+ density profiles from about 150 km up to about 500 km altitude (Kamalabadi et al. 2018). The ICON mission orbiting on a circular orbit at 27° inclination, only the geomagnetic equatorial region and mid-latitudes are monitored with FUV.

One of the main goals of the ICON mission is to understand the day-to-day climatology of the ionosphere, mainly driven by variations of atmospheric tides and atmospheric gravity waves that arise from lower atmosphere processes of tropospheric weather and solar forcing in the middle atmosphere. Disentangling the respective contribution of both forcings requires observations from both the lower atmosphere, the ionospheric peak region, which is the most important contribution to the observed variability, and observations at higher altitudes. The Data Product (DP) 2.5 of the ICON mission, which consists of full O^+ profiles of the nighttime ionosphere with a vertical resolution of a few km, provides an overview of the O^+ chemistry dynamics from 200 km to about 500 km altitude at a 12 s cadence. This unique dataset can be used for detecting and characterizing irregularities, such as small-scale ionospheric structures associated with scintillations observed from Global Navigation Satellite Systems (GNSS) data. In addition, peak density and height, N_mF_2 and h_mF_2 respectively, are representative of the state of the ionosphere, and remain important variables reflecting its state and variability.

A previous study performed by Wautelet et al. (2021) analyzed the first months of the ICON-FUV level-2 data product 2.5, comparing the peak-height characteristics with external data, such as the radio-occultation mission COSMIC-2 (C2) and ground-based ionosondes. The authors show that, using an appropriate exclusion filter for photoelectrons coming from the magneto-conjugate hemisphere, and if the background ionization remains larger than the threshold of 5×10^{11} m^{-3}, the mean peak density difference between ionosondes, C2 and ICON lies within 10% while the discrepancies in peak height were about 20 km with C2 and about 38 km with ionosonde datasets. This study was realized during the first year in orbit of ICON and several improvements have been included to the data processing so far, especially at the level-1 processing step with, notably, an improved capability for star detection and removal, a better background subtraction and an advanced code for computing the conjugate photoelectron contribution. A detailed study of Frey et al. (2023) (this collection) provides a full description of the FUV instrument and its in-flight performance, especially at the observational and calibration level. In this context, this paper provides an update of the results concerning the comparison, mainly at the peak-level, of O^+ density profiles provided

by ICON-FUV with electron density profiles inferred from COSMIC-2 and ground-based ionosondes.

2 Instruments and Methodology

The comparison work of Wautelet et al. (2021) assessed the performance of the O^+ density profiles measured from ICON-FUV. This previous work already made use of ionosondes and C2 mission as external data sources that have been well introduced in this reference; therefore we only remind here the essentials of each technique. The interested reader will find more details regarding these instruments in the aforementioned reference and in the recent study of Wautelet et al. (2022) who performed a similar study for the Extreme Ultra Violet (EUV) spectrograph onboard ICON. Note that, even though both EUV and FUV instruments aim at retrieving the O^+ density profile, they notably differ by the wavelengths used. Indeed, FUV makes the use of a single oxygen line at 135.6 nm while the measurement of two oxygen lines (a thick one at 83.4 nm and a thin one at 61.7 nm) is needed for EUV retrieval (Stephan et al. 2017). In addition, the EUV measurement method requires that the scene has to be illuminated by the Sun, i.e. during daytime, contrary to FUV measurement which monitors the radiative recombination of oxygen ions during nighttime. In that sense, both instruments provide complementary measurements to get a unique daytime and nighttime picture of the O^+ density over the concerned area.

2.1 ICON-FUV

The Far Ultraviolet Imager (FUV) onboard ICON is an imager of the limb and sub-limb ionosphere operating in two ultraviolet wavelengths: 135.6 nm and in the LBH band around 157 nm (Mende et al. 2017). The detector is divided into six different regions, called stripes, that are 3° wide and cover ±9° around the central view direction of the instrument. During nighttime, only the 135.6 nm channel is used and the level-1 calibrated images are inverted to produce six limb profiles at an observation cadence of 12 s, constituting the level-2 data product 2.5 (DP 2.5). Conversion from raw counts to level-1 radiances is a very important step of the data processing leading to DP 2.5 and we refer to Frey et al. (2023) for more details concerning the methodology.

The physics of the OI–135.6 nm nighttime emission consists of a main emission mechanism which is the radiative recombination of O^+ ions with ambient electrons. Another production mechanism is the mutual neutralization of atomic oxygen ions O^+ and O^- in the F-region, while loss is due to multiple scattering and absorption. All these mechanisms, which are detailed in Qin et al. (2015), are taken into account to invert the FUV radiance profiles to O^+ density profiles (Kamalabadi et al. 2018).

As previously mentioned, several improvements have been made since the previous study at the calibration and inversion levels. The list below briefly explains the major changes that directly impact the number and the quality of the comparisons:

- The background subtraction routine: the detector background is now monitored in each data sample allowing for a more accurate dynamic background subtraction.
- Photoelectron emission flag: a new variable was added since the version 4 of DP 2.5, which computes the percentage of the raypath passing through the F-peak illuminated in the conjugate hemisphere (Urco et al. 2021). If this value exceeds 10%, then the FUV data quality flag is reduced to 0.5, instead of 1 for good quality data.

- The star removal algorithm has been improved to address the issue of residual star signals contaminating the measurements that the previous algorithm failed to remove which was based on a simple median filter. The updated algorithm uses a deep neural network that has been trained on thousands of clean and starry measurement pairs to learn how to detect and remove the stars from measurements accurately. A specific convolutional neural network architecture known as U-net (Ronneberger et al. 2015) has been selected for this task, which has achieved the state-of-the-art performance in image segmentation and reconstruction problems (Lucas et al. 2018). The training dataset has been constructed by first collecting 2000 star-free nighttime profiles from the ICON FUV database, and then generating several starry versions of each profile by synthetically adding stars. The network takes as input a 6×256 array where the 256-pixel altitude profiles of 6 stripes are all provided at once, and the output is a 6×256 array of the star-removed version of the input.
- Improved quantitative on-orbit calibration with regular star observations (Frey et al. 2023).
- The DP 2.5 quality determination algorithm has been updated on version 4 to be more stringent in assigning a quality rating of 1. The update requires that measurements used by the algorithm have higher peak brightness and signal-to-noise ratio (SNR) values in order to qualify for a rating of 1.

Note that the new data acquisition flow is more conservative than for the previous versions, leading to less data associated with a quality flag of 1. It comes that, for the same period of time, less comparisons with C2 and ionosonde are available, but the latter have a better quality and consistency than before.

2.2 Radio-Occultation

Since June 2019, the six FORMOSAT-7/COSMIC-2 (further referred to as C2) satellites provide occultation measurements of the neutral and ionized atmosphere of the Earth (Straus et al. 2020). Like ICON, they are orbiting on slightly inclined circular low-earth orbits so that equatorial and mid-latitudes features are observed. For the ionospheric product, called "ionPrf", the quantity provided by C2 is the electron density N_e profile coming from radio-occultation of GNSS satellites which are orbiting at around 20,000 km altitude (medium-Earth orbit, or MEO). A typical occultation consists of GNSS phase observations that are calibrated to provide Total Electron Content (TEC) during the whole occultation path, which can take several minutes. A TEC value is associated to each tangent altitude, and the whole TEC profile is inverted to retrieve N_e, using an Abel-like inversion procedure, which is aided by integration of existing ionospheric data to prevent systematic artifacts due to the application of the classical method (Yue et al. 2011; Chou et al. 2017). Given the geometry of a typical GNSS occultation and its duration of several minutes, it should be highlighted that a C2 profile is not an instantaneous profile, unlike ICON-FUV or ionosondes which are able to give a 12 s snapshot for the first one, against a fully vertical profile every 2 or 3 minutes for the latter, depending on the facility.

The quality control of C2 profiles is the same as that implemented in Wautelet et al. (2021) and in Wautelet et al. (2022) where full details of the methodology can be found. Briefly, each N_e profile is iteratively fitted using a 4-parameter Chapman profile and is accepted as valid if the observed parameters N_mF_2 and h_mF_2, which also constitute the initial conditions of the algorithm, do not significantly differ from the modeled values:

$$N_e = N_m F_2 \, e^{\alpha \left[1 - \frac{(h - h_m F_2)}{H} - e^{-\frac{(h - h_m F_2)}{H}} \right]}$$

with N_e the electron density, N_mF_2 the electron density at the F_2 peak, α the Chapman parameter, h the altitude, h_mF_2 the altitude of the F_2 peak and H the scale height. Note that if observed N_mF_2 and h_mF_2 values are the initial conditions of this iterative process, the final modeled value will always differ from the observed ones.

Note that, like from previous studies, electron density profiles extracted from the C2 "IonPrf" product are still provisional data at the time of writing this study, and no error bar is provided with the density values. Based on the literature (Cherniak et al. 2021), we consider the C2 N_mF_2 standard deviation being equal to 0.5 MHz, further translated in electron number density, and that of h_mF_2 to 5 km.

2.3 Ionosonde

The vertical electron density profiles provided by the ground-based ionosondes have been reliably feeding the ionospheric community for decades, providing a truly vertical profile of the ionospheric bottomside above the facility location. An electromagnetic pulse is emitted vertically, then reflected back to the emitting station and finally received by the receiving antenna. Based on the basic principle of the time of flight computation of a radio signal in the range of 1 to 20 MHz, the ionosonde main basic observable is the ionogram, a graphical representation of the signal time of flight, translated into virtual height, as a function of the signal wavelength. The height is referred to as virtual because it supposes a free space propagation of the signal, which is never observed as the refractive index is not strictly equal to 1 in the atmosphere, producing multiple refractions before the signal is actually reflected. In the presence of a magnetic field in an ionized medium, the incoming signal is split into two components: the ordinary and the extraordinary rays, that are frequency separated by half the value of the gyrofrequency at the facility location and also visible on the ionograms (Piggot and Rawer 1978). The ionograms are then manually inspected and the ionogram trace, understood as the function associating each frequency step to a virtual height, is encoded into the SAO-Explorer software developed by Lowell Digisonde International (LDI). We then run the inversion routine, called NHPC (Huang and Reinisch 1996), included in SAO-Explorer software, to retrieve the electron density profile above the ionosonde station. Only the bottomside of the profile truly comes from the observations, as topside observations are not accessible with ionosonde measurements. Consequently, the topside part of the N_e profile provided by the NHPC routine is an extrapolation of the retrieved bottomside profile, based on climatological data.

The ionosonde network used in this work comprises several dozens of stations distributed worldwide and whose data can be freely accessed, e.g. via the FTP access provided by the National Oceanic and Atmospheric Administration (NOAA). The manual inspection and scaling of the ionogram is performed on all ionograms observed from 15 min before to 15 min after the time of the FUV-ionosonde conjunction, *i.e.* a space and time matching of observations (see below). Using a time series instead of a unique profile prevents misinterpretation of a particular ionogram, especially if its structure is more complex than the ones recorded before and after, and guarantees the understanding of the underlying physics. It is also a means to reduce the error on N_mF_2 as it follows a natural regular variation with time. The accurate scaling of the ionograms performed by trained scientists make the uncertainty on f_oF_2 very small, hence on N_mF_2 as well. As for the h_mF_2 uncertainty, it depends on the profile sharpness around the F-peak and has been fixed to the value of 5 km, which is estimated by visual inspection of numerous profiles and their sensitivity to little changes in their ionogram scaling.

We also refer the reader to Wautelet et al. (2021) and Wautelet et al. (2022) for more details concerning the ionosonde observations and the methodology applied to them.

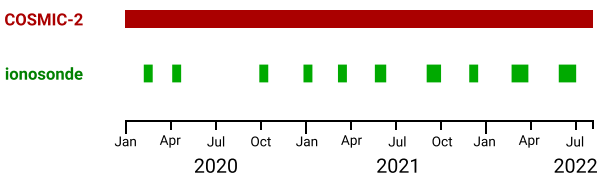

Fig. 1 Time coverage available for each external source

2.4 Comparison Methodology

The FUV, C2 and ionosonde observations have been compared to each other when both space and time conjunctions are met. Maximum distance of 500 km and maximum time difference of 15 min have been considered in this work. For C2 and FUV, the geographic position strongly changes with the tangent altitude considered, so that geolocation of the profile has been chosen to correspond to that of the F-peak, i.e. at h_mF_2. For the ionosonde, the location corresponds to the geographic location of the facility. Like for other ICON comparison studies (Wautelet et al. 2021, 2022), we proceed to a quality check allowing to select high quality profiles for all data sources. For FUV, it mainly consists in rejecting all profiles for which the inversion software did not flag the quality check equal to 1. This is the more restrictive criteria as a non negligible portion of FUV profiles do not meet that $quality = 1$ criteria. Note that the analysis of the number of available data showed that they are far less numerous with the new version 5 of the DP 2.5 product than with the version 3 used in the frame of the previous paper (Wautelet et al. 2021). Also, even if all profiles with $quality = 1$ are supposed to not correspond to cases where photoelectron contamination occur, we additionally exclude all measurements for which the solar zenith angle (SZA) at the magneto-conjugate point is lower than 110°, which still slightly decreases our sample size.

For C2, the internal quality check explained in the previous paragraphs and more detailed in Wautelet et al. (2021) is applied, with the same thresholds, being: $(N_mF_2\,obs. - N_mF_2\,fit) < 1 \times 10^{10}$ m^{-3}, $(h_mF_2\,obs. - h_mF_2\,fit) < 10$ km, $H \leq 100$ km and $\alpha \leq 2$. Similarly, C2 profiles with a smear value larger than 2200 km have been discarded from our dataset to keep a certain compatibility in the FUV geometric observation trace.

At last, the International Reference Ionosphere (IRI) 2016 model has been used to assess the expected difference resulting from the non-perfect colocation and synchronization of the profiles at the climatological level. This mean behavior is then subtracted from the observed differences in order to remove, on the average, the effects of the regular gradients. Therefore, we can state that the differences analyzed in this study can be considered as simultaneous and colocated at the IRI level, which inevitably underestimate the actual daily variability between the measurements.

The time intervals considered in this work differ from C2 to ionosonde stations, as exposed in Fig. 1. Indeed, the C2 constellation provides several thousands of profiles daily, while ionosonde data have to be manually scaled and validated, which requires a lot of work and explains the limited number of comparisons. The ionosonde comparisons were ideally performed every three months, in the aim of observing a large range of geomagnetic latitudes, local time and seasons without selecting a prohibitive number of profiles to validate manually. The size of the dataset reflects the manual intervention in the case of ionosondes: the total number of conjunctions, before any filtering, is 546794 for C2 and 1364 for the ionosonde dataset.

Table 1 Mean and standard deviation of ionospheric parameter differences between FUV and C2 and ionosondes (no outlier filter)

	N	$\Delta N_m F_2$ [m^{-3}]	$\Delta N_m F_2$ [%]	$\Delta h_m F_2$ [km]
FUV – COSMIC-2	339120	$-3.7 \times 10^9 \pm 5.4 \times 10^{11}$	10 ± 48	6 ± 24
FUV – ionosonde	1169	$9.0 \times 10^{10} \pm 2.2 \times 10^{11}$	33 ± 80	4 ± 35

3 F-Peak Parameters Results

Main comparison results rely on the F_2-peak parameters N_mF_2 and h_mF_2. Their differences, computed as "FUV minus external data" are detailed in Table 1 that will serve as a basis for a more detailed analysis. Maps of N_mF_2 and h_mF_2 differences are then presented for the COSMIC-2 analysis.

3.1 Summary Statistics

Results in Table 1 show that, with an average difference of about -3.7×10^9 m^{-3} for FUV-C2, the ΔN_mF_2 value is one order of magnitude smaller when considering the newest version of the ICON DP 2.5, the value found in the previous study (see Wautelet et al. 2021) being 9.6×10^{10} m^{-3} for both FUV-C2 and FUV-ionosonde comparison. In the new dataset, the mean difference is 9.0×10^{10} m^{-3} for the FUV-ionosonde comparison, which is approximately the same value than the one found the previous study. For ΔN_mF_2, the relative discrepancies are clearly reduced, decreasing from 55% (for C2) and 72% (ionosondes) to 10% and 33%, for C2 and ionosonde datasets respectively. Note however that the previous N_mF_2 conclusions took into account the dataset available at that time, and that the bias value was clearly decreased if an N_mF_2 threshold was considered. The conclusions related to peak height differences are similar: the differences between C2 and ICON-FUV are about three times less with the new file version, with 16 km before and 6 km in the present comparison. For ionosondes, a much yet better agreement is found, from 38 km previously to 4 km in the present comparison. Note that the previous conclusions in Wautelet et al. (2021) were obtained using the first seven months of the mission, i.e. from Nov. 2019 to Jun. 2020, while this work covers more than 2.5 years of data, including, notably, higher solar activity periods. Note also that the much closer mean values observed in this present comparison do not result from removing the conjugate photoelectron effects, as this was already done in the previous article, despite in a slightly different manner than in the present comparison.

Besides mean values which better agree with external sources, the variability, measured as the standard deviation, is not decreasing when considering absolute ΔN_mF_2 values: from 1.1×10^{11} in the previous comparison we get 5.4×10^{11} with the present dataset, meaning that the variability around the mean value is nearly five times larger. For the relative ΔN_mF_2 values, the variability is slightly reduced when considering C2 but slightly increased with the ionosonde comparison. The fact that absolute and relative differences lead to very different conclusions is most probably related to the very low solar activity prevailing in the former dataset, i.e. from November 2019 to June 2020. Under such solar minimum conditions, the N_mF_2 background is so low that relative difference values can easily reach several dozens (or hundreds) of percents, which was observed in Wautelet et al. (2021) results. Variability around the mean Δh_mF_2 values was, in the previous study, between 31

Table 2 Mean and standard deviation of ionospheric parameter differences between FUV and C2 and ionosondes (outlier filter applied)

	N	ΔN_mF_2 [m^{-3}]	ΔN_mF_2 [%]	Δh_mF_2 [km]
FUV – COSMIC-2	331476	$-3.3 \times 10^9 \pm 1.9 \times 10^{11}$	6 ± 33	7 ± 21
FUV – ionosonde	1072	$5.3 \times 10^{10} \pm 1.8 \times 10^{11}$	11 ± 32	7 ± 30

and 35 km and is now around 24 km, which is a substantial improvement for the new data release.

It is worth noting that N_mF_2 differences remain quite sensitive to extreme values, which is not the case for h_mF_2. If we are considering medians instead of mean values, the median of the relative N_mF_2 difference drops to 0% for the C2 dataset while it corresponds to 3% for ionosonde comparisons. In addition, Table 1 exhibits rather large variability with respect to the mean values, which would prove that the observed bias in density and height between FUV, C2 and ionosonde are not significant from a statistical point of view. A detailed analysis of several comparisons associated with very large discrepancies in either or both ΔN_mF_2 and Δh_mF_2 values reveals that statistics can be improved if we exclude some outliers from the analysis. We propose therefore to discard all comparisons corresponding to the following criteria:

- Absolute $\Delta N_mF_2 \geq 1 \times 10^{12}$ m^{-3}
- Relative $\Delta N_mF_2 \geq 200\%$
- Absolute $\Delta h_mF_2 \geq 100$ km

This filtering results in rejecting 3% and 8% of the data, for C2 and ionosonde datasets respectively. The updated statistics is given in Table 2. The outlier filtering only resulted in reducing the absolute variability of ΔN_mF_2 while other numbers do not significantly change. However, we point out that differences are now more consistent between C2 and ionosonde datasets, with mean and standard values more compatible. Finally, it comes that the slight positive N_mF_2 mean difference between FUV and external data sources can be considered to be less than or equal to 10% while peak height difference is 7 km, meaning that FUV is observing peak height at slightly larger altitudes and with a slightly enhanced density value than C2 and ionosondes.

Outlier filtering only removes very large discrepancies but large variability remains and has to be understood. Figures 2 and 3 summarize the different statistics appearing in Table 1, for C2 and ionosonde datasets respectively. Note that they correspond to the whole dataset, i.e. including the outliers discussed above. The top left panels 2a and 3a show the N_mF_2 scatter plots between FUV and C2 and ionosondes, respectively. Instead of representing each measurement individually, they rather represent a counting of the number of conjunctions falling within each hexagonal tile. From the color scale, we can rapidly understand that although the bulk of the data lies around the regression line $x=y$, numerous tiles are still located far from this line. Despite it is more obvious for the C2 dataset than with that related to ionosondes, the same observations can be drawn from the bottom left plots 2c and 3c showing h_mF_2 scatter plots. Top right plots, i.e. 2b and 3b show the dependency of the relative N_mF_2 difference to the absolute value, as measured by the external data source. Again, the conclusions are clearer with the C2 dataset but it seems evident that when N_mF_2 is very low, e.g. at mid-latitude during deep night conditions or under very low solar activity, relative differences can be very large, leading to what we called outliers above. In these plots

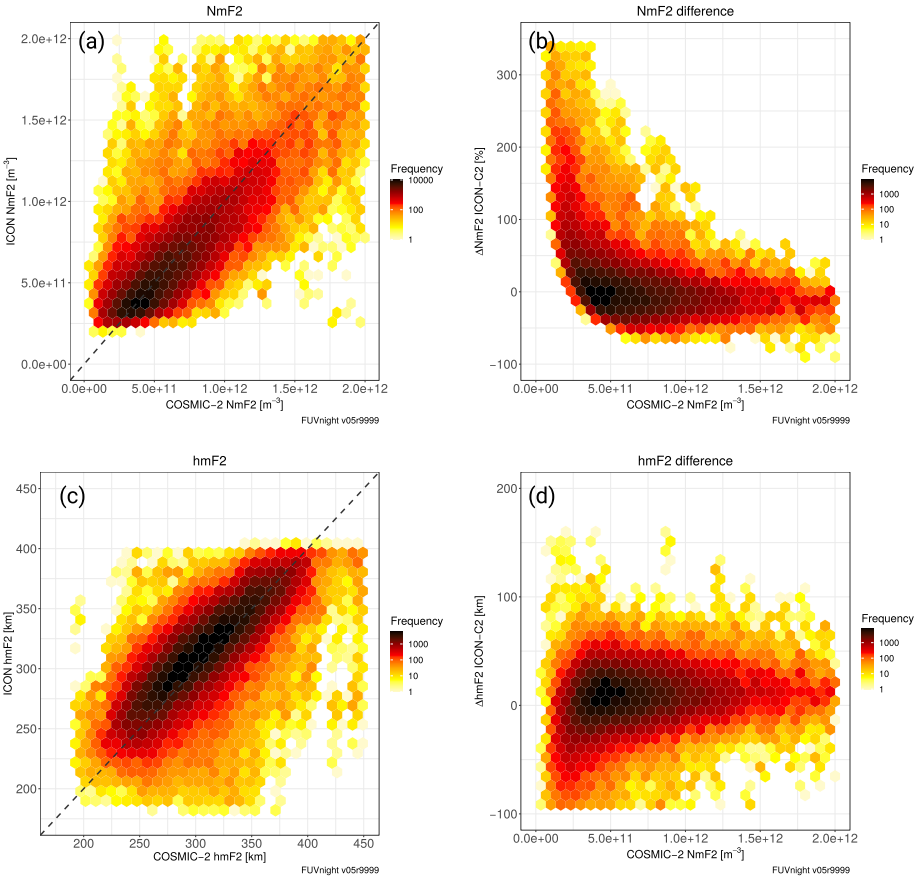

Fig. 2 FUV - C2 comparison: (a) scatter plot of N_mF_2, (b) relative ΔN_mF_2 as a function of the absolute N_mF_2 observed from C2, (c) scatter plot of h_mF_2, (d) Δh_mF_2 as a function of the absolute N_mF_2 observed from C2

we can infer that if we are considering a sufficiently large N_mF_2 value, say 5×10^{11} m^{-3}, it follows that the relative difference with the external data sources remains within 10% on average, with a variability not exceeding 40 to 50%. At last, we note from the last couple of Figs. 2d and 3d that the h_mF_2 difference is much less sensitive to the absolute N_mF_2 value than Δh_mF_2. It means that the value of h_mF_2 provided by FUV depends less on observational conditions, for instance the latitude or local time of the measurement.

For the sake of completeness, let us add that sensitivity tests have been carried out to assess the impact of the threshold used for the searching for conjunctions, being 500 km for the great circle distance at ionospheric height of 300 km and 15 min for the time interval. Such a study, already conducted in the paper of Wautelet et al. (2021), is reproduced here and shows similar results, stating that reducing the maximum search distance down to 100 or 200 km only reduces the ΔN_mF_2 mean bias and standard deviation values by 1% while the Δh_mF_2 values are similarly decreased by about 1 km, both in mean and standard deviation. On the other hand, the impact of reducing the 15 min time interval to smaller values is statistically null, as non significant increase nor decrease has been observed while making this value vary from 2 min to 15 min. In conclusion, because reducing such distance and time

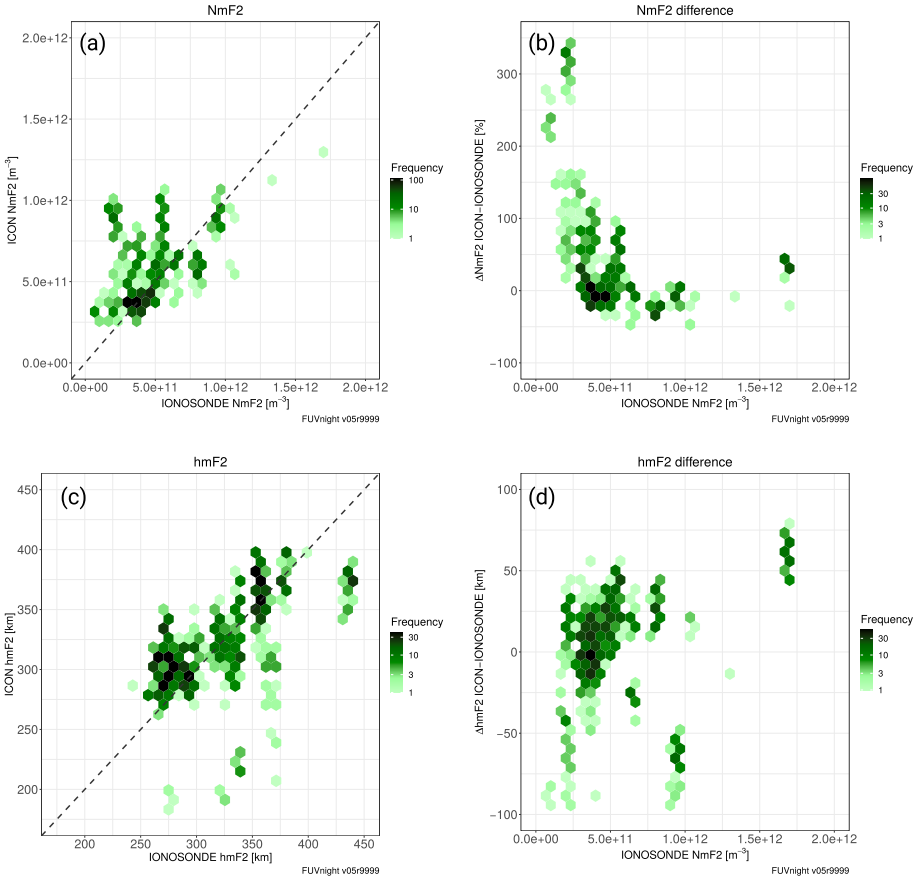

Fig. 3 FUV - ionosonde comparison: (a) scatter plot of N_mF_2, (b) relative ΔN_mF_2 as a function of the absolute N_mF_2 observed from ionosondes, (c) scatter plot of h_mF_2, (d) Δh_mF_2 as a function of the absolute N_mF_2 observed from ionosondes

difference parameters does not improve statistics but make the sample size much smaller, it has been chosen to maintain these thresholds to 500 km and 15 min.

3.2 COSMIC-2 Difference Maps

In addition to global statistics, we draw geographic maps of both ΔN_mF_2 and Δh_mF_2 to identify regions where mean differences are systematically larger or smaller than the global statistics. These maps have been produced for the COSMIC-2 dataset only, as the spatial distribution of the ionosonde network does not provide a global coverage.

From the analysis of Fig. 4a it comes that regions of enhanced and decreased ΔN_mF_2 are organized along the topology of the equatorial anomaly, with regions of increased differences mostly aligned with the ionization crests. The differences at the geomagnetic equator are significantly lower than around the crests, while mid-latitude conjunctions generally provide negative difference values. Note that such magnetic latitude effect seems to be less important over the Pacific ocean, where the maximum difference around the crests is clearly less visible than over the European and African longitude sector, for instance. For Δh_mF_2,

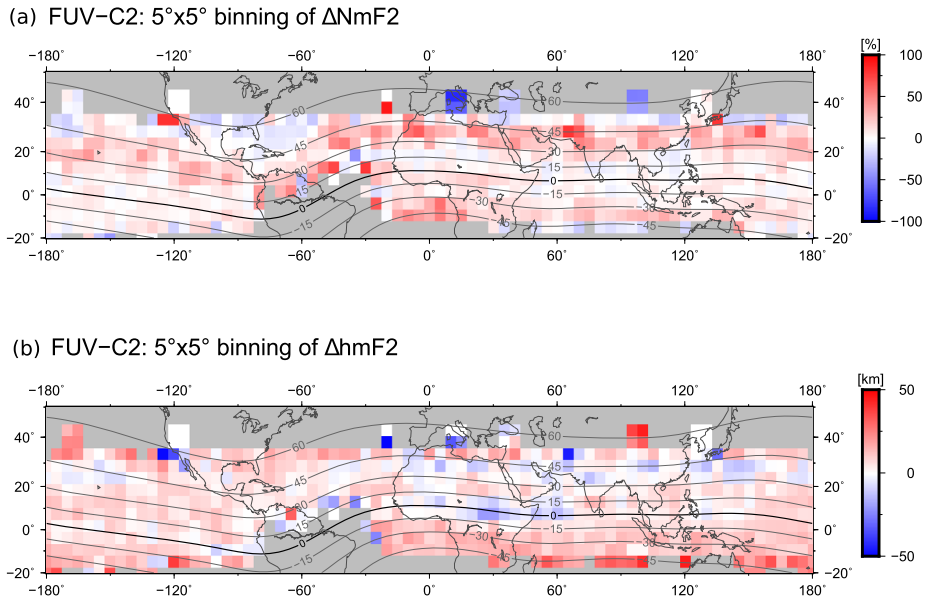

Fig. 4 FUV - C2 comparison. 5° × 5° bins of averaged relative $\Delta N_m F_2$ (a) and absolute $\Delta h_m F_2$ (b) values. Contour lines correspond to geomagnetic inclination, in degrees. Note the data gap around the South Atlantic Anomaly (SAA) which results from shutting down the instrument in order to protect it from energetic particles

the differences are not as well spatially correlated so that it seems difficult to infer any magnetic or geographic correlation, except that negative differences are more often found in the northern hemisphere than in the southern one.

Conclusions from Fig. 4 can be two fold: the magnetic pattern in $\Delta N_m F_2$ comes from the fact that FUV and C2 do not see the equatorial crests on the same way, meaning that radiative transfer related to FUV inversion has to be adjusted in order to decrease the density value at the peak when crossing strong latitudinal gradients of the crests. The second possibility is that more restrictions should be applied when dealing with radio-occultation data, since they do not correspond to vertical profiles. Indeed, a GNSS radio-occultation takes several minutes to be performed, in contrast to 12 s for ICON, and the orientation of the occultation plane (azimuth) can strongly differ from that of ICON. We can easily verify the latter hypothesis by restricting our analysis to conjunctions for which the orientation of both lines of sight is similar, meaning that the difference of the azimuth of the FUV line-of-sight and that of C2 profile, computed at the F-peak altitude, remain below a given value. In addition, let us also consider a maximum time difference smaller than 15 min, which most probably will decrease the effect of strong gradients related to the anomaly. Figure 5 depicts new maps of $\Delta N_m F_2$ and $\Delta h_m F_2$ while considering a maximum azimuth difference of 30° and a maximum time difference of 7.5 min, which is twice smaller than for the previous statistics.

The first observation while comparing Figs. 4 and 5 is that there are more empty cells, so that spatial coverage of the results is reduced. Indeed, the number of conjunctions included in Fig. 5 is 9960, against about 331000 for the whole dataset summarized in Table 2. Nevertheless, it is sufficient to notice that the effect of the ionization anomaly crests is no longer visible when taking into account the value of the azimuth, meaning that considering a similar geometry between radio-occultation and FUV greatly improves the degree of agreement

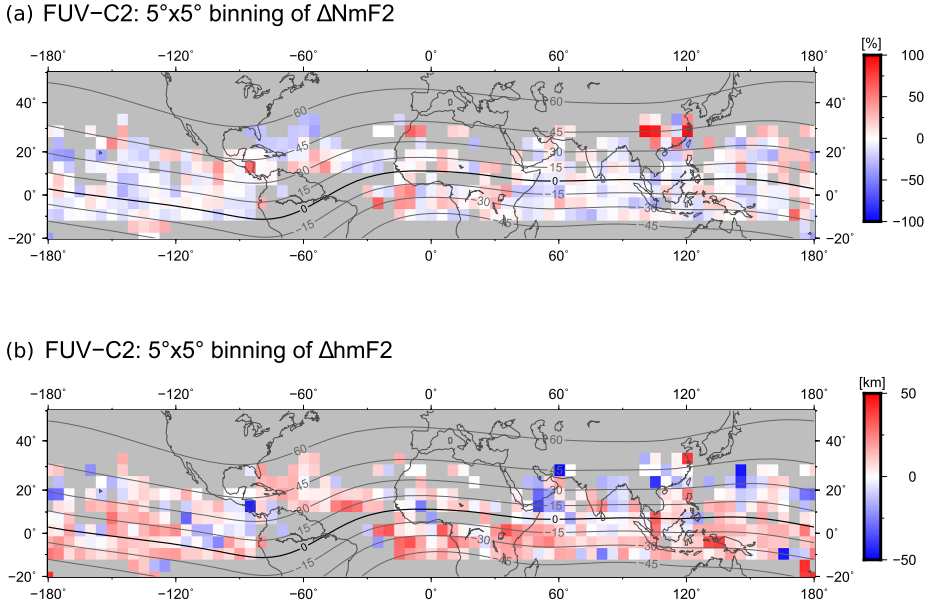

Fig. 5 Same caption as Fig. 4, except that it considers an azimuth filtering of 30° and a maximum time difference of 7.5 min

in terms of peak density, which is an important result. Let us also note that, as expected, the azimuth filtering does not change the peak height statistics and does only improve the density value comparison. In addition, considering such additional azimuth and time filtering also leads to more precise and accurate differences with respect to C2: mean $\Delta N_m F_2$ is now about -1% +/- 23%, against 6% +/- 33% in Table 2, while $\Delta h_m F_2$ is around 7 km +/- 20 km, against 7 km +/- 21 km. For the sake of completeness, we mention that taking an azimuth maximum difference of 20° instead of 30° does not significantly change these last results, the difference being approximately 1% for density and 1 km for peak height.

3.3 Complementary Results and Discussion

In the aim of understanding and reducing the variability in $\Delta N_m F_2$ and $\Delta h_m F_2$, we propose to investigate the special case of a given conjunction with C2 or ionosonde. In such a space and time match, numerous FUV profiles are compared against a unique C2 or ionosonde profile, meaning that the variability around a mean difference value does not only reflect the precision of the methods but also the natural variability of the ionosphere. As explained above, for each FUV profile and therefore each difference computation, the climatological O^+ and *Ne* difference in terms of IRI model is removed, so that the effect of the regular gradients can be considered as removed, from a climatological point of view. However, we do not remove the entire natural variability when applying the IRI model, and for two measurements measuring not exactly the same area at slightly different epochs, it is expected that some variability remains. Consequently, a natural question would be the following one: in a study dedicated to the assessment of the performance of the FUV instrument, would it not be more convenient to select, among the several dozens of measurements generally available for each conjunction, a single one that would best represent the conjunction?

The exercise has been performed for the two datasets, C2 and ionosonde, considering the four following possibilities to choose the "best" candidate for the conjunction: the closest in terms of N_mF_2, in terms of h_mF_2, in terms of geographic distance and in terms of time difference. Besides reducing the statistical power of the study – it divides the sample size by about 35 – we obtain a very slight reduction of the variability in two cases, when comparing with results from Table 2. Considering the FUV profile which is the closest to the C2 profile from the density point of view slightly improves the ΔN_mF_2 statistics, which become 5% +/- 29%, against 6% +/- 33% (see Table 2). The second slight improvement concerns the peak height, which is observed when considering the FUV profile for which the peak height is closest to that of the reference value. Instead of 7 km +/- 21 km as given in Table 2, the Δh_mF_2 statistics becomes 2 km +/- 16 km. The results given in this paragraph are related to the C2 dataset, but similar conclusions can be drawn from the ionosonde dataset.

We also establish that the mean differences and their standard deviation do not vary with time and therefore can be considered as a constant value reflecting the combined properties of the instrument, the measurement and the retrieval method. Figure 6 presents the time series of the mean daily difference of peak density (a) and peak height (b), together with the standard deviation of these values (subfigures c and d). Finally, Fig. 6e gives the daily absolute N_mF_2 value measured from C2, which can be considered as an indicator of the absolute ionization level.

Analysis of plots (a) to (d) from Fig. 6 shows very stable daily values, suggesting that the performance of FUV is stable with time and the changes of the ionization level. Indeed, the latter moderately fluctuated during the time interval considered, with very low level in 2019, 2020 and mid-2021 until the extremum in March – May 2022, when the Sun was the most active of the period. It is also interesting to note that the N_mF_2 difference is expressed in terms of relative values and that these values remain stable, regardless of the solar activity level. Therefore, if the absolute variability increases during high solar activity periods, the relative accuracy and precision is maintained. This is an important conclusion from this analysis, in addition to the fact that the step changes in the FUV high-voltage and in the background subtraction algorithm did not induce any break or linear trend in the time series.

In conclusion, we could summarize the main results from this study as follows. With respect to ground-based ionosondes and GNSS radio-occultation, we find that the accuracy of FUV N_mF_2 and h_mF_2 is about 6 to 10% (+/- 32%) and 7 km (+/- 25%) respectively. These numbers are very encouraging as the measurements arise from very different observation methods and retrieval algorithms and rely on the observations from one remote sensing instrument onboard a single platform. Because of the very small bias with respect to other techniques, it is therefore realistic to consider their inclusion in assimilative models. Beforehand, we first have to better understand the causes of the observed dispersion and ensure that it does not affect the whole profile. Under what specific conditions does strong variability appear? Is this because of an FUV-related issue or unrealistic external data sources? If a strong variability is observed for a given conjunction, is that the case for all FUV profiles participating to that conjunction or only a subset of them? In extension to this comparison work, is the FUV accuracy and precision stated here valid for the whole profile or do we also need to investigate the shape differences between FUV and external sources? Indeed, the latter question is of great interest in the frame of data assimilation: if only peak values are integrated into the models, so the statistics computed in this paper are valid and prove that, with certain care, they can be integrated. This work however does not guarantee the shape of the profile above and below the peak, so that scale heights can be very different from external data sources while peak values are compatible. In the next section, we will attempt to answer some of these questions using case studies, which pave the way to further studies dedicated to the full profile shape and their use in assimilation studies.

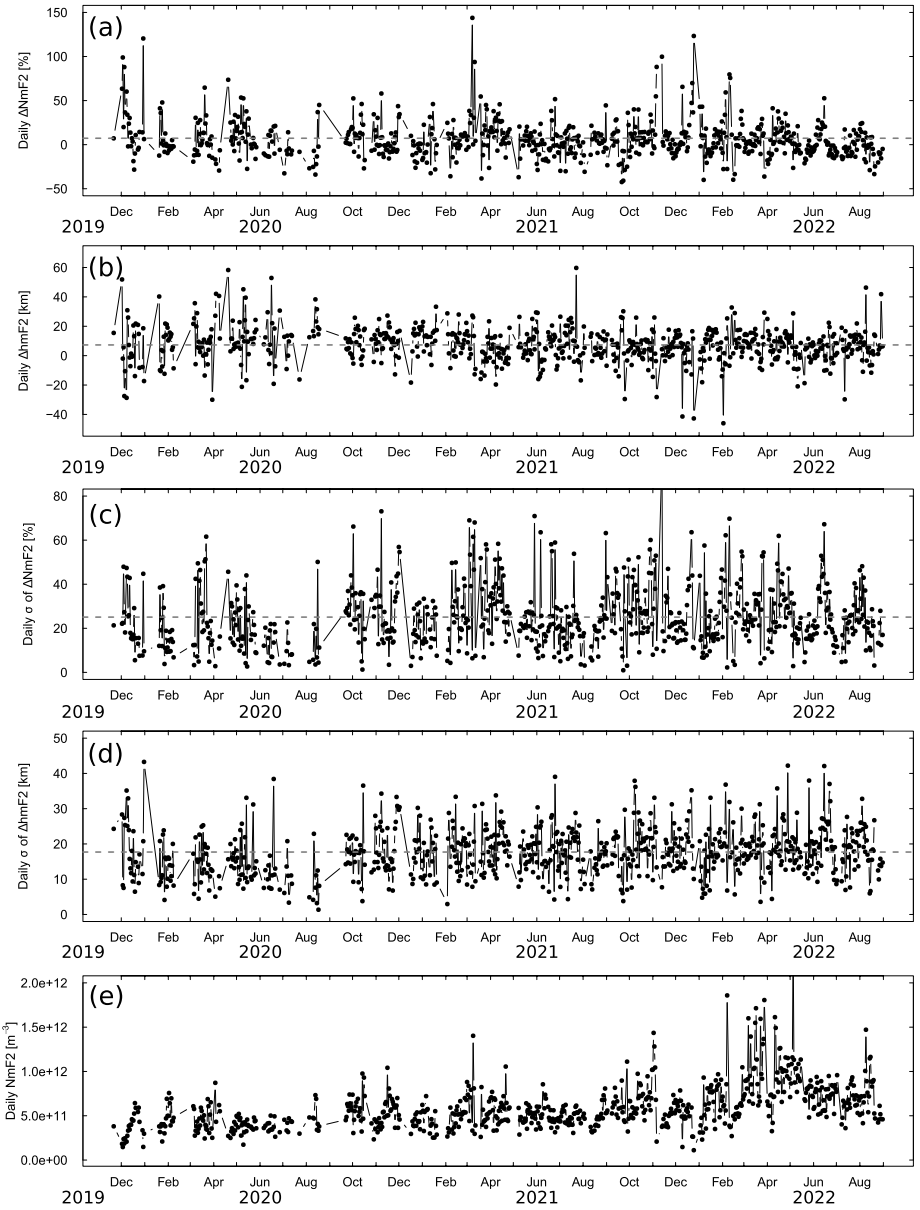

Fig. 6 Dec. 2019 – Aug. 2022 time series of (a) daily mean ΔN_mF_2 (in %), (b) daily mean Δh_mF_2 (in km), (c) daily standard deviation of ΔN_mF_2 (in %), (d) daily standard deviation of Δh_mF_2 (in km) and (e) daily mean absolute N_mF_2 observed by C2 (in m^{-3})

4 Focus on Variability: Case Study

To investigate why FUV and C2/ionosondes sometimes provide very different density and height of the peak, we first isolate conjunctions which provide moderate to large discrepancies in terms of ΔN_mF_2 or Δh_mF_2. We only selected a few of them, based on criteria (but

not only) such as $\Delta N_mF_2 > 200\%$ and $\Delta h_mF_2 > 70$ km, respectively. On the average, each conjunction gives between 2 and more than 50 FUV profiles, for a single profile coming from ionosondes or C2. Occasionally, two C2 or ionosonde profiles are available, which allows to better understand the context of the case and infer some conclusions concerning the variability on that particular conjunction.

On the 27 March 2022 (DOY 086/2022), two groups of conjunctions have been chosen to illustrate the variability in profiles and the complexity behind.

4.1 A Mid-Latitude Case

The first group shows moderate variability in Δh_mF_2, with discrepancies as large as 60 km and -70 km for two consecutive epochs. During less than 5 minutes, the 41 FUV profiles were located over Iran and Afghanistan, i.e. in the mid-latitude region, around 17 UT. Local time is between 22:00 and 22:30 in Spring, hence well after sunset, as verified by the solar zenith angle (SZA) of about 135°. Figure 7 shows three profiles out of these 41 cases to illustrate the recurrent features that we can point out as partially responsible for the variability in height differences. This conjunction is made up of two nearly colocated C2 profiles. Figure 7a is a typical example of a FUV-C2 comparison under relatively low ionization background. We can clearly identify the main F-peak which is correctly measured by FUV, together with a second and a third peak in the bottomside of the profile. Along time and stripes, the relative intensity for these peaks vary and if a secondary peak provides larger density than the actual F-peak, we observe a large discrepancy in peak height. This is what happened in the case of Fig. 7a, where Δh_mF_2 is about 70 km lower than that observed by C2. A couple of minutes later, the secondary peaks tend to disappear and we obtain profile comparison similar to that shown in Fig. 7b and c, the latter corresponding to the same FUV measurement as Fig. 7b but with the other C2 profile. The subfigures b and c show that a perfect match is obtained with both C2 profiles, which are very consistent despite the 70° azimuth differences between them.

The origin of multiple bumps or peaks in FUV profiles is probably linked to a weak ionization background which prevents the star removal algorithm to efficiently discern regions of high brightness. Because FUV profiles are inverted data, they also result from regularization process that has to manage with weak inputs with important relative errors. Regularization methods aiming at simultaneously penalizing spurious variations and improving the conditioning of the problem can also sometimes smooth real variations.

4.2 On the Equatorial Anomaly Crests

The second conjunction analyzed in this work has been identified based on its large ΔN_mF_2 values between FUV and C2, which always exceed 100%. This conjunction case corresponds to local time between 21:00 and 22:00 observed around the northern crest of the geomagnetic equator (between 16 and 20° MLAT) in the Pacific sector, at about 128° E longitude. Figure 8 shows three examples of the profile comparison, with the panel (a) corresponding to the beginning of the conjunction, while panels (b) and (c) correspond to its end. In panel (a), even though the FUV O^+ retrieval precision is high, especially around the peak altitudes (i.e. small error), the absolute peak density is at least twice that of C2. In addition, let us remark the relatively good agreement between the shapes of the FUV and C2 profiles, although the FUV one is narrower, suggesting a smaller scale height at the peak altitude. From the middle panel (b), which was recorded less than three minutes later than (a), the error bars are still very small but the shape of the FUV profile completely

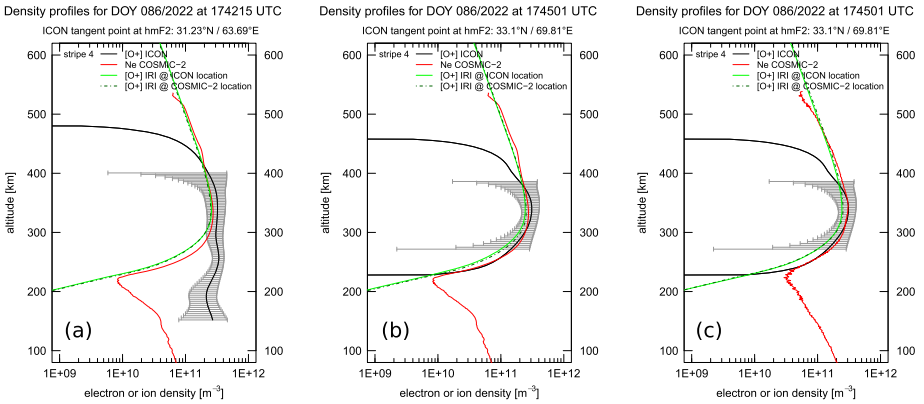

Fig. 7 Conjunction FUV-C2 on DOY 086/2022 between 17:42 and 17:45 UT. For the whole conjunction, LT varies from 21:57 to 22:31 to while MLAT ranges from 24° to 26°. Three examples of O^+ density profiles derived from FUV (black) compared with the electron density profiles coming from COSMIC-2 (red) and the O^+ density profiles provided by IRI (dashed green lines). More specifically, IRI is computed at both FUV and C2 locations to appreciate the climatological difference due to the not perfect synchronization and geolocation between FUV and C2 profiles compared. Error bars are only provided for FUV and are depicted as horizontal bars on the FUV profile. Note that two different C2 profiles correspond to (b) and (c) cases, with very consistent profile and peak characteristics

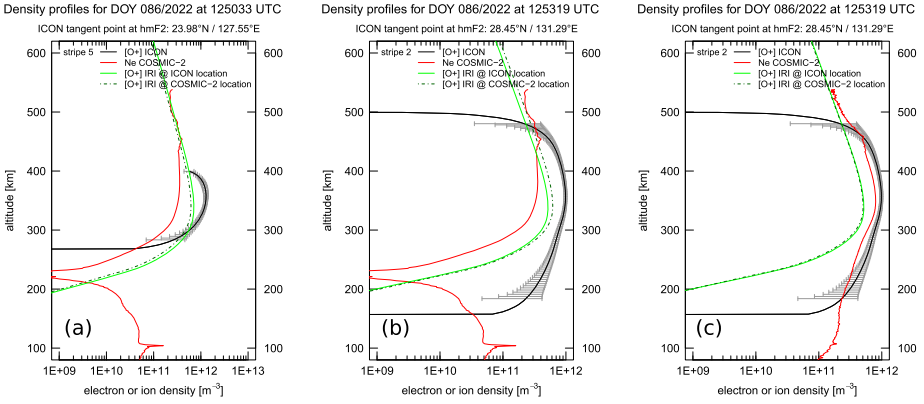

Fig. 8 Conjunction FUV-C2 on DOY 086/2022 between 12:50 and 12:54 UT. For the whole conjunction, LT varies from 21:20 to 21:44 to while MLAT ranges from 15° to 20°. The remaining description is similar to the caption of Fig. 7

changed, revealing a much larger density at lower altitudes. This bottomside feature does not correspond to the C2 profile, especially at the altitude where its minimum is observed around 220 km. Even though it has no impact on the h_mF_2 retrieval, density differences of several orders of magnitude with external data sources can be problematic when considering the profile as a whole, and not only the peak characteristics. However, this conjunction also has the chance to be colocated and synchronized with another C2 profile, whose comparison with the FUV profile of Fig. 8b is shown on the right panel (c). This unexpected result shows that both peak density and height match very well the C2 profile, which is only a few hundreds of km and several minutes from the other C2 profile, well within the pre-determined

criteria defining a conjunction. This situation is the opposite to that of previous conjunction, where the two C2 profiles were fully consistent with each other. In such a situation, it is therefore difficult to state that a given profile is more reliable than the other one, and so the related FUV ΔN_mF_2 and Δh_mF_2 values. For the sake of completeness, let us mention that these huge differences are not explained by an azimuth difference between FUV and the respective C2 profiles: ICON azimuth value (353°) lies nearly exactly in the middle of the two C2 ones, being around 300° and 35°.

This case study only covers a very limited number of cases but the situations depicted here have been encountered numerous times. From our manual inspection of multiple matches, and as illustrated in the two above cases, we can summarize the different phenomena that led to unexpected variability on peak characteristics. First, the presence of multiple peaks, or bumps, in the profile data which, in certain circumstances, can be interpreted as the maximum density value, even though observed at very low or high altitudes. Second, the presence of very weak ionization level, for instance in mid-latitude regions under low solar activity period, is often but not always correlated to profiles with multiple bumps. Third, even in the absence of several bumps, some profiles can quickly change from relatively narrow to rather broad profiles, sometime leading to very different peak height values. An issue with very fast changing shapes is that the scale height at low or high altitudes can dramatically change in a couple of minutes or degrees, even though it is not the case of the main peak parameters, with a direct consequence on all applications that ingest the whole FUV profiles. At last, let us point out that over the crests of the geomagnetic equator, it seems to be extremely challenging to get airglow and radio-occultation that perfectly agree due to the extreme variability in space and time induced by this ionospheric feature. Much care should be taken when using FUV or C2 profiles for which the crests make a substantial contribution to the integrated values.

5 Summary and Conclusion

We present an update of the performance assessment of the nighttime O^+ limb profiles measured by the ICON-FUV instrument. The time interval considered in this study is extended in comparison with the previous study (Wautelet et al. 2021), and several important improvements have been implemented at both calibration and inversion levels. Conjunctions with electron density profiles coming from the COSMIC-2 radio-occultation mission and ground-based ionosondes show that, on the average, FUV density and height are compatible with the external data sources at the peak level. More specifically, the peak density N_mF_2 observed from FUV shows slightly larger values by only 6% and 11% than C2 and ionosonde values respectively. The peak altitude h_mF_2 obtained from the ICON FUV data is also slightly larger than that measured by C2 and ionosondes by 7 km, this value being identical for the two methods based on radio signals. The comparison datasets have been further investigated in terms of the variability around the mean behavior which showcases a full compatibility with external data sources, at the F-peak level. It is shown that N_mF_2 differences between FUV and C2 can be significantly reduced by restricting our analysis to observations having similar azimuth values. This azimuth-dependent effect is most probably due to the large difference of the observational conditions between the two methods: FUV provides nearly instantaneous snapshots of the 135.6 nm emission while C2 results from the integration of several minutes of GNSS occultation, and this effect leads to very different profiles when large space and time gradients are present. An evidence of the sensitivity of radio-occultation method to the gradient crossing lies in the very different C2 profiles we

obtained from a same conjunction case, i.e. within 15 min and 500 km radius around FUV. We therefore invite the reader to pay attention to the fact that the inconsistency, at the peak level, can arise not only from FUV variability but also from the C2 inconsistency so that the geometry of the different data sources is really worth investigating before assimilating or merging the profiles together. Another main conclusion from this study is that some large discrepancies have also been observed at altitudes well below the main F-peak, where FUV sometimes provides double or triple peaks in the O^+ density profiles. Probably due to weak ionization conditions, these profiles are however flagged as *quality* = 1 and can correspond to N_mF_2 and h_mF_2 values which are compatible with external data sources, despite a large disagreement at low altitudes. Understanding and mitigating the variability of FUV profiles, especially on the bottomside, will certainly help in providing more reliable profiles which would be used in assimilative models or studies. Finally, let us remind that FUV DP 2.5 came with no particular requirement regarding its accuracy with respect to existing ionospheric data. However, we proved that peak N_mF_2 and h_mF_2 values are close to external datasets with differences of less than 10% and 7 km, respectively, which is quite remarkable given the difference in the nature of the observation methods considered. From that point of view, FUV succeeds at the accuracy level while internal precision would most probably be improved while considering the different aspects discussed in this study.

Acknowledgements The authors are grateful to the ICON Science Team for the interesting discussions and collaboration throughout these first three years in orbit.

Funding Gilles Wautelet, Benoît Hubert, and Jean-Claude Gérard acknowledge financial support from the Belgian Federal Science Policy Office (BELSPO) via the PRODEX Program of ESA. Benoît Hubert is supported by the Belgian Fund for Scientific Research (FNRS). ICON is supported by NASA's Explorers Program through contracts NNG12FA45C and NNG12FA42I.

Data Availability ICON data are processed in the ICON Science Data Center at University of California, Berkeley, and are available at https://icon.ssl.berkeley.edu/Data.

Declarations

Competing Interests The authors declare to have no conflict of interest or competing interest.

References

Cherniak I, Zakharenkova I, Braun J, Wu Q, Pedatella N, Schreiner W, Weiss J-P, Hunt D (2021) Accuracy assessment of the quiet-time ionospheric F2 peak parameters as derived from COSMIC-2 multi-GNSS radio occultation measurements. J Space Weather Space Clim 11:18. https://doi.org/10.1051/swsc/2020080

Chou MY, Lin CCH, Tsai HF, Lin CY (2017) Ionospheric electron density inversion for global navigation satellite systems radio occultation using aided Abel inversions. J Geophys Res Space Phys 122(1):1386–1399. https://doi.org/10.1002/2016JA023027

Frey HU, Mende SB, Meier RR, Kamaci U, Urco JM, Kamalabadi F, England SL, Immel TJ (2023) In flight performance of the Far Ultraviolet instrument (FUV) on ICON. Space Sci Rev 219. https://doi.org/10.1007/s11214-023-00969-9

Huang X, Reinisch BW (1996) Vertical electron density profiles from the digisonde network. Adv Space Res 18(6):121–129

Kamalabadi F, Qin J, Harding BJ, Iliou D, Makela JJ, Meier RR, England SL, Frey HU, Mende SB, Immel TJ (2018) Inferring nighttime ionospheric parameters with the far ultraviolet imager onboard the ionospheric connection explorer. Space Sci Rev 214(4):70. https://doi.org/10.1007/s11214-018-0502-9

Lucas A, Iliadis M, Molina R, Katsaggelos AK (2018) Using deep neural networks for inverse problems in imaging: beyond analytical methods. IEEE Signal Process Mag 35(1):20–36. https://doi.org/10.1109/MSP.2017.2760358

Mende SB, Frey HU, Rider K, Chou C, Harris SE, Siegmund OHW, England SL, Wilkins C, Craig W, Immel TJ, Turin P, Darling N, Loicq J, Blain P, Syrstad E, Thompson B, Burt R, Champagne J, Sevilla P, Ellis S (2017) The Far Ultra-Violet imager on the ICON mission. Space Sci Rev 212(1):655–696. https://doi.org/10.1007/s11214-017-0386-0

Mende SB, Frey HU, England SL, Immel TJ, Eastes RW (2022) Time delay integration imaging of the nighttime ionosphere from the ICON observatory. Space Sci Rev 218:61. https://doi.org/10.1007/s11214-022-00928-w

Piggot WR, Rawer K (July 1978) U.R.S.I. Handbook of ionogram interpretation and reduction. Revision of Chaps. 1-4. Technical Report UAG-23A, World Data Center A for Solar-Terrestrial Physics Warsaw, Poland. Revision Adopted by U.R.S.I. Commission III

Qin J, Makela JJ, Kamalabadi F, Meier RR (2015) Radiative transfer modeling of the OI 135.6 nm emission in the nighttime ionosphere. J Geophys Res Space Phys 120(11):10116–10135. https://doi.org/10.1002/2015JA021687

Ronneberger O, Fischer P, Brox T (2015) U-net: convolutional networks for biomedical image segmentation. In: Navab N, Hornegger J, Wells WM, Frangi AF (eds) International conference on medical image computing and computer-assisted intervention – MICCAI 2015: 18th International Conference, Munich, Germany, October 5–9. Lecture notes in computer science 9351:234–241, Springer, Cham. https://doi.org/10.1007/978-3-319-24574-4_28

Stephan AW, Korpela EJ, Sirk MM, England SL, Immel TJ (2017) Daytime ionosphere retrieval algorithm for the Ionospheric Connection Explorer (ICON). Space Sci Rev 212(1):645–654. https://doi.org/10.1007/s11214-017-0385-1

Straus P, Schreiner W, Santiago J, Talaat E, Lin C-L (March 2020) FORMOSAT-7/COSMIC-2 TGRS Space Weather Provisional Data Release 1. Technical report, NOAA, USAF and NSPO

Urco JM, Kamalabadi F, Kamaci U, Harding BJ, Frey HU, Mende SB, Huba JD, England SL, Immel TJ (2021) Conjugate photoelectron energy spectra derived from coincident FUV and radio measurements. Geophys Res Lett 48(23):e2021GL095839. https://doi.org/10.1029/2021GL095839

Wautelet G, Hubert B, Gérard J-C, Immel TJ, Frey HU, Mende SB, Kamalabadi F, Kamaci U, England SL (2021) First ICON-FUV nighttime NmF2 and hmF2 comparison to ground and space-based measurements. J Geophys Res Space Phys 126(11):e2021JA029360. https://doi.org/10.1029/2021JA029360

Wautelet G, Hubert B, Gérard J-C, Immel TJ, Sirk MM, Korpela E, Stephan AW, Mende SB, England SL, Erickson PJ (2022) Comparison of ICON-EUV F-peak characteristic parameters with external data source. Space Sci Rev 218:62. https://doi.org/10.1007/s11214-022-00930-2

Yue X, Schreiner WS, Lin Y-C, Rocken C, Kuo Y-H, Zhao B (2011) Data assimilation retrieval of electron density profiles from radio occultation measurements. J Geophys Res Space Phys 116:A03317. https://doi.org/10.1029/2010JA015980

Publisher's Note Springer Nature remains neutral with regard to jurisdictional claims in published maps and institutional affiliations.

Springer Nature or its licensor (e.g. a society or other partner) holds exclusive rights to this article under a publishing agreement with the author(s) or other rightsholder(s); author self-archiving of the accepted manuscript version of this article is solely governed by the terms of such publishing agreement and applicable law.